Nanoscale

PAPER

View Article Online
View Journal | View Issue

Cite this: *Nanoscale*, 2023, **15**, 15279

Effect of the effective refractive index on the radiative decay rate in nanoparticle thin films†

Manuel Romero, Juan Ramón Sánchez-Valencia, Gabriel Lozano * and Hernán Míguez *

In this work, we theoretically and experimentally study the influence of the optical environment on the radiative decay rate of rare-earth transitions in luminescent nanoparticles forming a thin film. We use electric dipole sources in finite-difference time-domain simulations to analyze the effect of modifying the effective refractive index of transparent layers made of phosphor nanocrystals doped with rare earth cations, and propose a correction to previously reported analytical models for calculating the radiative decay rate. Our predictions are tested against an experimental realization of such luminescent films, in which we manage to vary the effective refractive index in a gradual and controllable manner. Our model accurately accounts for the measurements attained, allows us to discriminate the radiative and non-radiative contributions to the time-resolved photoluminescence, and provides a way to rationally tune the spontaneous decay rate and hence the photoluminescence quantum yield in an ensemble of luminescent nanoparticles.

Received 10th July 2023,
Accepted 31st August 2023

DOI: 10.1039/d3nr03348a

rsc.li/nanoscale

Introduction

Luminescence is essentially a quantum phenomenon that depends on the probability of an excited electron decaying to the ground state by emitting a photon, which is mainly determined by the set of energy levels of the material. In addition to the intrinsic structural properties of the emitter, the optical environment influences the radiative decay probability (Γ_{rad}) through the local density of optical states (LDOS).[1] Drexhage demonstrated this photonic effect by measuring the photoluminescence (PL) dynamics of an emitter as a function of its position relative to an interface.[2,3] Since then, a wide variety of optical materials made of dielectrics and metals, nanostructured at the scale of the targeted photon wavelength, have been used to manipulate the LDOS and thus modify the PL of nanomaterials, including semiconductor nanocrystals, organic molecules or rare earth (RE) phosphor nanoparticles.[4–9,10] However, the simplest approach to changing the LDOS of a light source is to modify the refractive index (n) of the medium in which it is embedded, which can easily be done in simple systems such as nanoparticle dispersions by using solvents with different values of n.[11–16] Indeed, an almost cubic dependence of Γ_{rad} on the solvent refractive index has been observed, which has been classically explained by the use of local field cavity models.[17–20] Although this theoretical formalism can be applied to any luminescent nanoparticle, including dye-doped polymer beads or semiconductor quantum dots, most reported examples involve phosphor nanoparticles. In fact, Senden *et al.* used $LaPO_4$ nanocrystals doped with Ce^{3+} or Tb^{3+} with a size of ~4 nm in various solvents and confirmed the validity of these models for luminescent nanoparticles in suspension.[11] Besides, cavity models have also been employed to explain variations in Γ_{rad} in concentrated suspensions.[15,17,20] In particular, the dependence of Γ_{rad} in Eu^{3+}-doped Y_2O_3 nanocrystals with particle sizes between 7 nm and 12 nm has been successfully described by replacing the solvent refractive index surrounding the emitting nanoparticles by the effective refractive index of the suspension (n_{eff}), estimated assuming that the nanocrystals occupy 23% of the volume.[16] Nevertheless, the interparticle distance in a film decreases to almost zero, allowing for near-field interparticle interactions that lead to deviations from cavity models, making necessary to introduce an explicit dependence with the particle filling fraction (c_{np}).[18] To the best of our knowledge, a study of the dependence of Γ_{rad} on n_{eff} in thin films made of luminescent nanoparticles has never been carried out, despite its relevance to the large number of applications in which solids made with nanoemit-

Institute of Materials Science of Seville, Spanish National Research Council – University of Seville, C. Américo Vespucio 49, 41092 Seville, Spain.
E-mail: g.lozano@csic.es, h.miguez@csic.es

†Electronic supplementary information (ESI) available: Mie calculations of the scattering cross section of the luminescent nanoparticles (Fig. S1); ellipsometry data (Fig. S2); Inokuti–Hirayama model and time-dependent PL measurements (eqn (S1)–(S2) and Fig. S3); bi-exponential fitting parameters (Fig. S4); absolute PLQY values (Fig. S5); non-radiative rates (Fig. S6); relationship between PLQY and Grad for the Inokuti-Hirayama model (eqn (S3)); radiative, non-radiative and Eu–Eu rate for the Inokuti–Hirayama model (Fig. S7). See DOI: https://doi.org/10.1039/d3nr03348a

ters are employed, including imaging, sensing, signalling, colour conversion, or quantum technologies.[21–23]

Here we present a thorough theoretical and experimental analysis of the variation of the emission properties of a model luminescent nanoparticle as a result of being part of thin films with gradually variable n_{eff}. To this end, we combine LDOS calculations with a detailed photophysical characterization of the fabricated phosphor nanoparticle thin films. In particular, we model Γ_{rad}, find deviations between finite-difference time-domain (FDTD) simulations and the cavity models, and propose a correction which accounts for the c_{np} of the films. A careful analysis of the time-dependent PL and the PL quantum yield (PLQY) of the films allows the estimation of Γ_{rad} from measurements of $GdVO_4$:Eu^{3+} nanoparticle-based films of variable refractive index, providing an experimental validation of the proposed model. As a result, we demonstrate a simple method to tune the Γ_{rad} in phosphor thin films, which holds great promise for any application where luminescent nanomaterials are integrated as coatings, including sensing, labelling or colour conversion in displays or lamps.

Results and discussion

Theoretical calculation of the radiative decay rate

The radiative decay rate of a randomly oriented two-level emitter under the dipole approximation is given by:[1]

$$\Gamma_{rad} = \frac{\pi\omega|\boldsymbol{p}|^2}{3\hbar\varepsilon_0 n^2}\mathrm{LDOS}(\boldsymbol{r},\omega) \quad (1)$$

where $\boldsymbol{p}$ is the dipole moment of the quantum emitter, ω is the angular frequency of the emitted photon, ε_0 is the dielectric permittivity of vacuum, n is the refractive index of the medium, $\hbar$ is the reduced Planck's constant and $\boldsymbol{r}$ is the position of the dipole. In turn, the LDOS is proportional to the trace of the dyadic Green function $\left(\overleftrightarrow{\boldsymbol{G}}\right)$ according to:

$$\mathrm{LDOS}(\boldsymbol{r},\omega) = \frac{2\omega n^2}{\pi c^2}\mathrm{Tr}\left[\mathrm{Im}\left\{\overleftrightarrow{\boldsymbol{G}}(\boldsymbol{r},\boldsymbol{r},\omega)\right\}\right] \quad (2)$$

being c the speed of light in vacuum. In this way, LDOS is completely determined only by the magnetic permeability μ, n and the geometry of the system. The analytical calculation of Γ_{rad} through the LDOS in arbitrary structures is not straightforward, and in the case of a random dense packing of nanoparticles the problem becomes computationally burdensome as it involves the resolution of large linear systems.[24] For this reason, FDTD simulations combined with dipole sources are typically used to calculate the enhancement of Γ_{rad} associated with the presence of complex photonic structures.[25–27] Specifically, simulating the radiated power from an electric dipole antenna allows the calculation of Γ_{rad} as:[1]

$$\Gamma_{rad} = \frac{4|\boldsymbol{p}|^2}{\hbar\omega|\boldsymbol{d}|^2}\langle P\rangle(\boldsymbol{d},\boldsymbol{r},\omega) \quad (3)$$

where $\boldsymbol{d}$ is the dipole moment of the antenna and $\langle P\rangle$ is the mean power radiated by the dipole. In the case of randomly oriented emitters, three orthogonal orientations of the dipole antenna should be calculated and averaged. This quantum classical connection provides an efficient way to calculate radiative rates in arbitrary structures, which we will use to assess the effect of interparticle interactions in nanoparticle thin films. We calculated Γ_{rad}/Γ_0 -Γ_0 being the radiative rate in vacuum- for an emitter in the center of a nanoparticle with a diameter of 50 nm and a refractive index n_{np} suspended in a homogeneous medium with a refractive index n_{ext}, as shown in the schematic of Fig. 1a. The results are shown in Fig. 1b. We performed a series of simulations for n_{np} = 2.0 and calculated the relative difference Δ between the FDTD results and the exact solution of the problem given by $\overleftrightarrow{\boldsymbol{G}}$.[28] Good agreement is found when comparing simulated and analytical results, with random values of Δ less than 16%, associated with the numerical error of the FDTD method. In what follows, we make use of a modified version of the analytical expression reported by Duan and Reid for the Γ_{rad} of a single nanoparticle in suspension in the limit where the size of the nanoparticle is much smaller than the wavelength:[17]

$$\Gamma_{rad} = \Gamma_0\mathrm{Tr}\left[\mathrm{Im}\left\{\overleftrightarrow{\boldsymbol{G}}\right\}\right] = \Gamma_0 n_{ext}\left(\frac{3{n_{ext}}^2}{2{n_{ext}}^2 + {n_{np}}^2}\right)^2 \quad (4)$$

In our case, as an effective medium is considered, the medium refractive index (n_{ext}) shall be substituted by n_{eff}, constituting what we will refer to as the particle in effective medium (PEM) model. To account for interparticle interactions in a film, we then calculated the $\langle P\rangle$ of an electric dipole antenna placed at the center of a nanoparticle thin film with a moderate filling fraction (c_{np} = 30%) for two different values of the n_{np} -specifically n_{np} = 1.7 and 2.0- as a function of the n_{eff}, as shown in Fig. 1c. Note that n_{eff} of any material is a function of the indices of its individual constituents (n_i) and their respective loading fraction (c_i). In the case of a nanoparticle thin film, we have:

$$n_{eff} = F(n_{np}, c_{np}, n_{pore}, c_{pore}) \quad (5)$$

where n_{pore} and c_{pore} are the refractive index and the filling fraction of the material filling the pores between the nanoparticles. The function F can be given by any of the existing effective medium approximations (EMA). In this work, the Bruggeman effective medium approximation was used because it describes media with moderate and high values of c_{np}.[29] In addition, the n_{eff} of the film was modified in the simulation either by changing n_{pore} or by introducing nanoparticles with a lower n_{np} into the film. Note that, unlike other proposed models,[18] our approach can be extended to composite films consisting of more than one type of nanoparticles. Our simulations consider a layer of thickness 500 nm, but the results are not dependent on this parameter. For the moderate c_{np} under consideration, an almost identical dependence of Γ_{rad} on the refractive index to that expected for a nanoparticle suspended in a homogeneous medium with an index n_{eff} (see

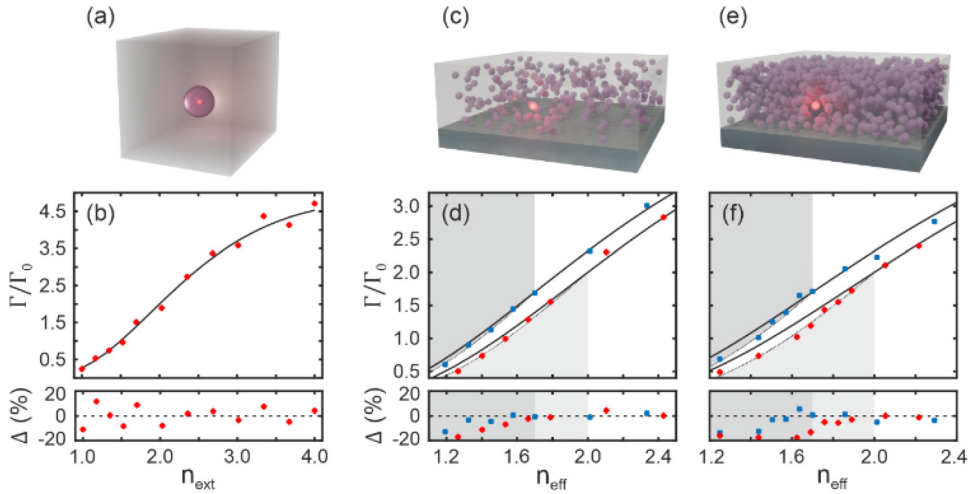

Fig. 1 (a) Schematic of a nanoparticle of refractive index n_{np} suspended in a homogeneous medium of refractive index n_{ext}. (b) Simulated radiative rate (dots) of an emitter placed at the center of a particle suspended in a medium of refractive index n_{ext}. Calculations obtained from the dyadic Green function are shown as a solid line for comparison. The relative difference between theory and simulations is shown in the lower panel. (c and e) Schematic of a system made of nanoparticles of refractive index n_{np} with a loading fraction c_{np} = 30% (c) and c_{np} = 64% (e). (d and f) Simulated radiative rates of an emitter placed at the center of a nanoparticle near the center of the films as a function of the effective index of the medium in which the emitter is embedded are shown as dots whereas the calculations given by the dyadic Green function of a particle suspended in the same effective medium are shown as solid lines. Red dots correspond to nanoparticles with n_{np} = 2.0, while the blue dots correspond to nanoparticles with n_{np} = 1.7. All the calculations were performed for nanoparticles with a radius of 25 nm. Our correction to the cavity model is plotted as a dotted line in (d) and (f).

Fig. 1d) is found, as already reported for nanocrystals in suspension.[11] However, slight discrepancies appear when increasing the refractive index difference between n_{np} and that of the effective medium when $n_{eff} < n_{np}$, suggesting that the influence of particle interactions not considered in the EMA is overlooked in eqn (4). More specifically, deviations between the Γ_{rad} predicted by FDTD calculations and those estimated by the particle suspended in an effective medium model show up, especially when $n_{eff} < n_{np}$. This is explicit in simulations performed for a densely packed nanoparticle thin film with c_{np} = 64%, sketched in Fig. 1e, whose results are plotted in Fig. 1f. Note that the asymmetric behaviour of the system with respect to the sign of the refractive index difference between n_{eff} and n_{np} stems from Mie theory. An intrinsic asymmetry in scattering efficiency is observed as a function of the refractive index difference between the particle and the surrounding medium (see Fig. S1†). Additionally, our results serve to establish an approximate filling fraction range where the PEM model can be applied. In this context, attending to the reduced level of deviation from the PEM for c_{np} = 30%, we can estimate the validity of the PEM for $c_{np} < 30\%$ for the refractive index values considered. We propose a correction in the expression of Γ_{rad} given by eqn (4) to account for the effect of interparticle interactions in layers made of luminescent nanoparticles. This correction is only valid when $n_{eff} < n_{np}$ and takes the following form:

$$\Gamma_{rad} = \Gamma_0 \cdot \left(\frac{n_{eff}}{n_{np}}\right)^{c_{np}} \cdot \mathrm{Tr}\left[\mathrm{Im}\left\{\vec{\vec{G}}_{PEM}\right\}\right] \quad (6)$$

where c_{np} is given by the sum of each individual nanoparticle filling fraction $c_{np,i}$ in a composite, and $\vec{\vec{G}}_{PEM}$ is the vacuum-normalized dyadic Green function in the PEM model. If the homogeneous refractive index is replaced by n_{eff} and take the limit where the size of the nanoparticles is much smaller than the wavelength, our expression gives:

$$\Gamma_{rad} = \Gamma_0 \cdot n_{eff} \left(\frac{n_{eff}}{n_{np}}\right)^{c_{np}} \left(\frac{3{n_{eff}}^2}{2{n_{eff}}^2 + {n_{np}}^2}\right)^2 \quad (7)$$

that fairly reproduces the dependence of Γ_{rad} on n_{eff} for all sets of simulations (see dotted lines in Fig. 1d and f). Note that our correction does not include any empirical constants as fitting parameters. Instead, it involves only physical quantities: n_{np}, c_{np} and n_{eff}. Moreover, it respects the bulk limit, *i.e.* when the nanoparticles are embedded in a medium with the same index ($n_{eff} = n_{np}$, as in a dense layer), $\Gamma = n_{np}\Gamma_0$.[18] Also, in the limit of low filling fraction, *i.e.* $c_{np} \to 0$, our correction recovers the expression of a particle in a homogeneous medium (eqn (4)).

A case study: $GdVO_4$:Eu^{3+}-based nanoparticle thin films

Phosphor nanoparticles were chosen as the experimental probe to demonstrate the effect of n_{eff} on Γ_{rad}. Phosphors are key materials for efficient light generation due to their chemical and thermal stability combined with a high PLQY.[30] In particular, we employ $GdVO_4$:Eu^{3+} nanoparticles with an approximate size of 50 nm (see Fig. 2a), which exhibit bright PL with a narrow PL emission peak at λ_0 = 620 nm when excited in the UV.[30] These nanoparticles allow the preparation of thin films (see Fig. 2b) that are uniform in thickness and transparent in the visible spectral region. In addition, these nanophosphor films feature reduced light scattering,[30] which allows n_{eff} to be determined using standard spectroscopic techniques. In fact,

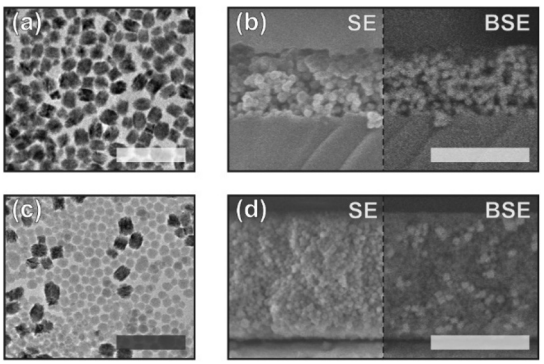

Fig. 2 (a) TEM image of $GdVO_4$:Eu^{3+} nanoparticles. (b) Secondary (SE) and backscattered electrons (BSE) SEM images of a thin film made of $GdVO_4$:Eu^{3+} nanoparticles. (c) TEM image of $GdVO_4$:Eu^{3+} and SiO_2 nanoparticles, the latter being less contrasted. (d) SE and BSE images of a cross section of a thin film with a ratio of $GdVO_4$:Eu^{3+} to SiO_2 nanoparticles of 0.22. The TEM scale bars correspond to 200 nm, while the SEM scale bars correspond to 500 nm.

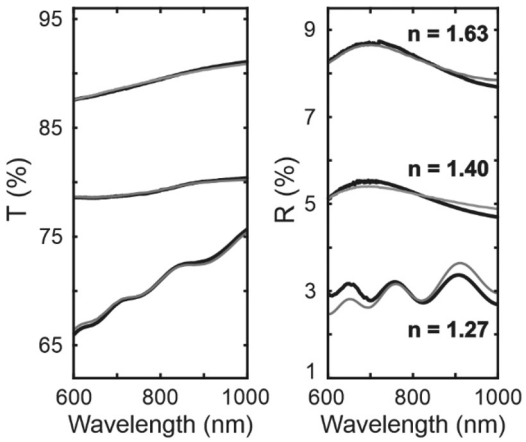

Fig. 3 Experimental transmittance and reflectance spectra (black lines) and corresponding theoretical fits (grey lines). The angle of incidence of the unpolarized light is 30°. The lower lines correspond to a composite made of $GdVO_4$:Eu^{3+} and SiO_2 nanoparticles, the middle lines correspond to a $GdVO_4$:Eu^{3+} film and the upper lines correspond to a $GdVO_4$:Eu^{3+} film embedded in PMMA. The calculated refractive index of each material is also shown.

$GdVO_4$:Eu^{3+} thin films have an n_{eff} = 1.4 in the visible range, as we will show later. To change the film index in a controlled way, in one approach, we prepare nanocomposite thin films made of $GdVO_4$:Eu^{3+} and SiO_2 nanoparticles of similar size (see Fig. 2c). By including as building blocks nanoparticles with a composition of lower refractive index (1.46 *vs.* 1.75) we manage to controllably reduce n_{eff}. Also, we take advantage of the accessible porosity of the films and infiltrate their void space with polymers, thus changing the refractive index of interstices between nanoparticles (n_{pore}), hence increasing n_{eff}. So, in order to access a wide range of n_{eff} values, uniform films with thicknesses ranging from 250 nm to 2 μm with different SiO_2 to $GdVO_4$:Eu^{3+} c_{np} were prepared (see Fig. 2d) and then infiltrated with polymers: poly(methyl methacrylate) (PMMA, n = 1.49), polyvinyl alcohol (PVA, n = 1.48) or polydimethylsiloxane (PDMS, n = 1.40). Although the mixing of phosphor and SiO_2 nanoparticles results in different film thickness values due to variations in particle concentration dispersion, this parameter does not change Γ_{rad}, as mentioned above. Please note that the approach herein taken allows tuning n_{eff} in a broad range, overcoming a common limitation in the study of photonic effects on the Γ_{rad} of luminescent nanoemitters.

We extract the optical constants of our films by fitting the spectral dependence of the ballistic transmittance (T) and the specular reflectance (R) measured for different angles of incidence, following a procedure that has been thoroughly described before (see the Methods section).[31] In Fig. 3 we show the experimental R and T (black lines) and their corresponding theoretical fits (grey lines) using the Bruggeman EMA. The calculated filling fraction of the only-nanophosphor films is c_{np} = 55 ± 5%. To account for the observed variation in the n_{eff} of the samples prepared in different batches, a certain spread was included in the calculated c_{np} and 55% was taken as the nominal value. The obtained n_{eff} of the $GdVO_4$:Eu^{3+} films was n_{eff} = 1.40, which becomes n_{eff} = 1.63 when the air voids are infiltrated with PMMA, or n_{eff} = 1.60 when infiltrated with PDMS. Besides, we prepared composite films in which the SiO_2 to $GdVO_4$:Eu^{3+} volume ratio was varied as 1 : 5, 1 : 1.25 and 1 : 0.22, resulting in n_{eff} = 1.37, 1.32, 1.27, respectively. Effective refractive index values were further confirmed by ellipsometry (see Fig. S2†).

Eu^{3+} cations in our $GdVO_4$ nanoparticles exhibit four main atomic transitions, giving rise to the measured PL spectra shown in Fig. 4a. Although these transitions are associated with the $^5D_0$ excited state, they can exhibit different values of Γ_{rad} depending on the probability of the transition to the ground state. LDOS affect atomic transitions depending on their magnetic or electric nature.[32] We calculated the ratio of the total intensities of the forced electric dipole FED and magnetic dipole (MD) transition[32] and obtained a mean value of 11.49. Thus, the FED transitions are dominant in our system ($^5D_0 \rightarrow {}^7F_2$, $^7F_3$, $^7F_4$), allowing us to focus on the electric part of the LDOS. In addition, different radiative rates may be associated with a given atomic transition if, for example, the LDOS varies in the spatial region where Eu^{3+} cations are distributed within a nanoparticle. To shed light on this possible effect, in Fig. 4b we have used LDOS theory applied to spherical systems[28] to calculate analytically the ratio of the Γ_{rad} of an emitter placed near the surface (Γ_S) of a nanoparticle (n_{np} = 1.75) with radius R_{part}, suspended in a homogeneous medium with refractive index n_{ext}, to the Γ_{rad} of an emitter located at the centre of the same nanoparticle (Γ_C). From these calculations, it can be concluded that Γ_{rad} varies by less than 5% within the volume of our nanoparticles, given the particle size and the n_{ext} values considered. Therefore, LDOS variations within a nanoparticle are neglected in our analysis, as expected for nanoparticles which are much smaller than the wavelength.

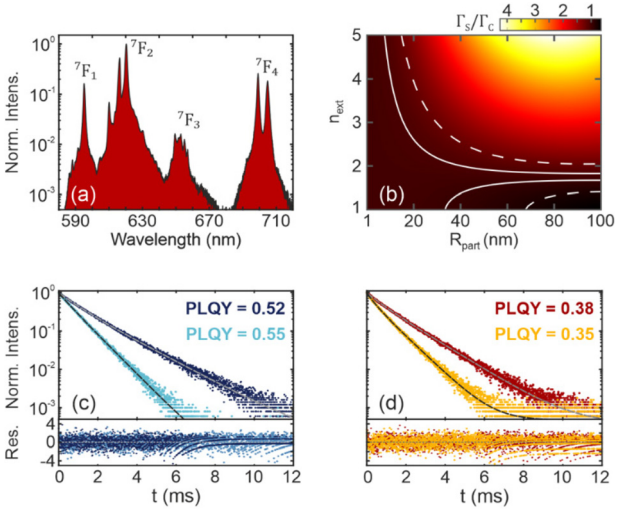

Fig. 4 (a) Experimental PL spectra of a $GdVO_4$:Eu^{3+} nanoparticle film excited at 300 nm. The fundamental level of each Eu^{3+} transition is shown. (b) Calculated ratio between the radiative rate near the surface (Γ_S) and at the center (Γ_C) of a spherical nanoparticle with refractive index n_{np} = 1.75 for λ_0 = 620 nm, as a function of the nanoparticle radius (R_{part}) and the refractive index surrounding the nanoparticle (n_{ext}). Solid (dashed) lines enclose the set of parameters for which the variation between Γ_S and Γ_C is less than 5% (20%). (c and d) Experimental photoluminescence decay for a $GdVO_4$:Eu^{3+} film before (dark blue symbols) and after (light blue symbols) PMMA infiltration (c), and for a composite film made of $GdVO_4$:Eu^{3+} and SiO_2 nanoparticles before (red symbols) and after (yellow symbols) PVA infiltration (d). Fits are shown as black and grey curves. The residuals of the fits are shown in the lower part of the plots. Measured quantum yield values are also indicated in the upper part.

Time-dependent PL measurements were performed for the prepared samples to study the depopulation of $^5D_0$ level after UV excitation (λ_{exc} = 300 nm) and hence, obtain Γ_{rad} (see Fig. 4c and d). This is given by the sum of the four main Eu^{3+} radiative transition rates. PL intensity $I(t)$ is typically fitted using a bi-exponential model according to:

$$I(t) = I_0 \cdot [w_1 \exp(-\Gamma_{tot,1} \cdot t) + w_2 \exp(-\Gamma_{tot,2} \cdot t)] \quad (8)$$

where $\Gamma_{tot,i}$ with i = 1 or 2, is the total decay rate of the ith component -sum of $\Gamma_{rad,i}$ and non-radiative decay rate ($\Gamma_{nr,i}$)-, w_i is its corresponding weight and I_0 the initial PL intensity. Fits can be found in Fig. S3.† The bi-exponential model has been reported to explain time-dependent PL measurements in RE-doped nanocrystals. It suggests that it is not possible to assign a single intrinsic rate to all the cations in our films. Although it has been shown that cross-relaxation and concentration quenching play an important role in the analysis of the time-dependent PL,[33] the physical origin of the bi-exponential model remains rather unclear. Some works attributed this behaviour to different local environments of RE cations in the lattice, assuming that different non-radiative decay paths occur near the surface or in the bulk of the nanoparticle,[34,35] while others explained the deviation from the single exponential behaviour according to an energy transfer process between the crystal host and cation acceptor.[36] Within this latter hypothesis, Inokuti and Hirayama developed a donor–acceptor energy transfer model,[37] which has been used to explain PL decay in RE-doped materials.[38–40] It succeeded in fitting experimental decays of YVO_4:Eu^{3+} nanocrystals,[38] explaining the deviation from mono-exponential decay by attending to Eu–Eu multipolar interaction. However, although this model gave significantly better results than the single exponential model, the calculated bi-exponential fits were superior in our case (see Fig. S3†). Fig. 4c and d show measured PL decay spectra of the only-nanophosphor film (Fig. 4c) and the composite film with the highest amount of SiO_2 (Fig. 4d), before and after polymer infiltration. Bare films show similar average lifetime values (see Fig. S4†), although they have different effective indices (1.40 *vs.* 1.27). Furthermore, polymer infiltration leads to a significant decrease in the lifetime for both cases while the PLQY hardly increases or even decreases (see Fig. S5†), which cannot be explained by the modification of the optical environment alone. Therefore, the observed lifetime reduction results both from a modification of Γ_{rad} according to eqn (7) and the emergence of new non-radiative decay channels. We measure the PLQY, which can be defined as the ratio between radiative and total decay rates in order to extract Γ_{rad} from Γ_{tot}. In a general case, PLQY is given by the ratio between the radiative and total -sum of radiative and non-radiative- decay rates as:

$$\mathrm{PLQY} = \frac{\Gamma_{rad}}{\Gamma_{tot}} = \frac{\Gamma_{rad}}{\Gamma_{rad} + \Gamma_{nr}} \quad (9)$$

On the one hand, $\Gamma_{rad,1} = \Gamma_{rad,2}$ in the biexponential model because the LDOS does not vary within a RE-doped nanoparticle. Considering this, PLQY can be expressed in the bi-exponential model -see the ESI† for a relationship between PLQY and transition rates in the Inokuti–Hirayama model- in the following manner:

$$\mathrm{PLQY} = \Gamma_{rad}\left(\frac{w_1}{\Gamma_{tot,1}} + \frac{w_2}{\Gamma_{tot,2}}\right) \quad (10)$$

In this way, the combination of absolute PLQY measurements (see Fig. S5†) and PL decay fits enables a general way to discriminate the radiative contribution to the total rate, allowing us to calculate Γ_{rad} for films with different effective refractive index, as shown in Fig. 5. Experimental results indicate that Γ_{rad} follows an almost cubic dependence with n_{eff}. Note that the data in Fig. 5 are obtained using the biexponential model. However, our conclusions are independent of the model used (see Fig. S7†). Specifically, our results further support that Γ_{rad} in nanoparticle films deviates from the dependence expected from the PEM model (gray solid line) and rather behaves like the correction proposed in eqn (7) (black dashed dotted line). The strong dependence of Γ_{rad} with the n_{eff} reveals the enormous potential of refractive index engineering to increase the emission rate of luminescent films which can be key in Li–Fi (Light Fidelity) applications.[41] In fact, the Γ_{rad} increases from 350 to 550 Hz with the infiltration

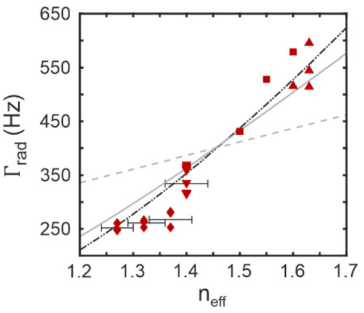

Fig. 5 Calculated radiative decay rate (Γ_{rad}) for films with different values of the effective refractive index (n_{eff}). The grey dashed line corresponds to linear scaling as expected for emitters in a homogeneous medium, the grey solid line is given by the LDOS calculation of a nanoparticle suspended in a medium with n_{eff}, and the black dashed dotted line corresponds to the proposed correction. Error bars are included to account for the variation in nanoparticle filling fraction between similar samples. Square points correspond to composite-based films, while triangles correspond to only-phosphor-based films.

of PMMA, achieving a 57% increase when the n_{eff} goes from 1.40 to 1.63.[42] Although the PLQY is slightly higher when our nanophosphor films are embedded in polymers (from 0.52 to 0.55 with PMMA, see Fig. S5,† the improvement is less than expected (22%) considering the change in Γ_{rad}. To explain this, we also extracted Γ_{nr} (see Fig. S6 and S7†) and found that the non-radiative contributions increased when the nanophosphor films were modified, either by adding SiO_2 nanoparticles or by infiltrating the films with polymers. We attribute this to a change in the chemical environment of the nanocrystals or their surface properties, inducing new non-radiative decay channels for the deexcitation of Eu^{3+} transitions that partially counterbalance the enhancement of Γ_{rad}. It highlights the relevance of limiting the impact of non-radiative decay channels in order to fully exploit the benefits of photonic effects in phosphor nanoparticles. These results support the use of our model to engineer the radiative rate of generic luminescent nanoparticle films, *i.e.*, not only including those made of phosphor nanoparticles, as we have just demonstrated with the case study presented, but also others like dye-doped polymer beads or semiconductor nanocrystals.

Conclusions

We have demonstrated the feasibility of the FDTD method to calculate changes in the Γ_{rad} due to the optical environment, and applied this general method to elucidate the impact of the refractive index in luminescent nanoparticle thin films. We have found deviations from the PEM model as the film filling fraction increases, which have been accounted for in a correction based solely on physical parameters. The first experimental study of the dependence of the Γ_{rad} of luminescent nanocrystals on the n_{eff} of a thin film is also presented, with a detailed analysis of PL decays and PLQY measurements, which allowed us to discriminate between radiative and non-radiative processes taking place in our samples. The high level of agreement between theoretical and experimental results points at the refractive index modification in nanoparticle thin films as a straightforward and simple method to enhance or inhibit the radiative decay rate of light-emitting materials. Although fundamental in nature, our results hold great promise for applications where control of the emission rate is critical, such as lighting, medical imaging, or optical wireless communications.

Methods

Simulations

FDTD simulations were carried out using commercial software (Ansys©, Lumerical FDTD). All the calculations used a uniform discretization with 2 nm mesh and absorbing boundary conditions (PML).

For the case of a particle in a uniform medium, a simulation domain of $(0.4 \times 0.4 \times 0.4)$ μm^3 was used and an electric dipole was placed in the centre of the particle. A single orientation of the dipole was used, given the spherical symmetry of the system.

In the nanoparticle thin film simulations, simulation domain was of $(1.0 \times 1.0 \times 1.1)$ μm^3 and the thickness of the film was 500 nm. For the low filling fraction film, a random set of spheres was generated, while special code developed by others[43] was used to generate a random close-packing of spheres. In these cases, three simulations of three orthogonal dipole orientations were performed and averaged to account for random dipole orientation. The dipoles were placed in the centre of a particle which is near the geometric centre of the film, which is chosen as a representative point of the film.

Synthesis of $GdVO_4$:Eu^{3+} nanocrystals, nanocomposite and thin films

Synthesis of $GdVO_4$:Eu^{3+} nanophosphor was performed following a solvothermal method previously reported.[44] Eu^{3+} concentration was fixed at 10% ($Gd_{0.9}VO_4$:$Eu_{0.1}^{3+}$). Briefly, uniform NPs were obtained through homogeneous precipitation reaction from the RE precursors and sodium orthovanadate in EG/water mixture at 120 °C. Polyacrylic acid (PAA) was added during the synthesis as functionalization agent. As a result, sized-controlled nanophosphors with colloidal stability dispersed in methanol were attained.

Nanocomposite dispersion by directly adding certain volume of LUDOX® TMA colloidal silica (34 wt%) suspension in water to the $GdVO_4$:Eu^{3+} suspension in methanol. Various suspensions with distinct SiO_2/$GdVO_4$ ratios were prepared and sonicated for 15 min to avoid aggregation.

Thin films were prepared by spin coating over fused silica substrates and annealed at 500 °C for 1 h to remove organic binders and improve $GdVO_4$:Eu^{3+} crystallinity.

Infiltration with polymers was performed by drop casting in all cases. In the case of PMMA, a 5 wt% solution in anisole was deposited over the thin film, and no heating was applied

to evaporate the solvent. For PVA, a 1 wt% solution in water was deposited and heated at 70 °C for 1 h to evaporate the solvent. PDMS was prepared by mixing 9 parts in weight of Sylgard 184 prepolymer and 1 part of curing agent. After vigorously mixing, the mixture was placed in vacuum to remove air bubbles. After the infiltration process, the sample was heated to 90 °C for 1.5 hours to enable polymerization.

Photoluminescence measurements

Emission spectra and time-dependent PL intensity were measured with an Edinburgh FLS1000 spectrofluorometer under an excitation of λ_{ex} = 300 nm. Time-dependent PL measurements were registered for the most intense Eu^{3+} emission band at 620 nm using a MCS method and a pulsed xenon lamp at 40 Hz repetition rate. Time window was set to 20 ms with 4000 channels and a maximum count number of 5000.

PL decay fittings were obtained from weighted least squares minimization. Poisson weights w_i were considered, being the objective function h to minimize:

$$h = \sum_{i}^{N} w_i^2 \cdot \left(S_i - S_i^*\right)^2 \quad (11)$$

where S_i^* correspond to the experimental data, and S_i is the result of the fittings which depends on the fitting parameters -see eqn (8)- and N is the number of data points. The weights are given by the following expression:

$$w_i = \frac{1}{\sqrt{S_i^*}} \quad (12)$$

Finally, the chi-square parameter (χ^2) can be calculated as h/N.

Quantum yield measurements

Absolute quantum yield measurements were performed in a Hamamatsu Photonics equipment consisting in an integrating sphere connected to a photo spectrometer and to a xenon lamp as excitation source. This equipment is able to count the number of absorbed and emitted photons, estimating the PLQY.

Refractive index determination

Refractive index determination was carried out by theoretically fitting R and T spectra measured for three different incident angles in a commercial Cary 5000 UV-Vis-NIR coupled to a double goniometer (UMA accessory). The transfer matrix method is used to theoretically calculate R and T at the same angles of incidence and then to minimize the difference between experimental data and calculations by varying the refractive index of the film and its thickness. Our model accounts for a small fraction of scattering given by the experimental 1-R-T, as our samples are non-absorbing in the visible. It also allows for some variation in film thickness to account for thickness inhomogeneity in thick films. Finally, a commercial variable angle spectroscopic ellipsometer (VASE) from J.A. Woollam Co., Inc. was used to confirm the refractive index data.

Abbreviations

EMA	Effective medium approximation
FDTD	Finite-difference time-domain
LDOS	Local density of optical states
PEM	Particle in effective medium
PL	Photoluminescence
PLQY	Photoluminescence quantum yield
RE	Rare earth

Data availability

Data for this paper are available at Digital CSIC at https://doi.org/10.20350/digitalCSIC/15509. The code for estimating the effective refractive index of an arbitrary layered optical material may be found at **https://github.com/Multifunctional-OpticalMaterials-Group**.

Conflicts of interest

There are no conflicts to declare.

Acknowledgements

This project has received funding from the European Research Council (ERC) under the European Union's Horizon 2020 Research and Innovation Programme (NANOPHOM, grant agreement no. 715832), from the BBVA Foundation Leonardo Grant for Physics Researchers 2023, and from MCIN/AEI/10.13039/501100011033 by European Union NextGeneration EU/PRTR under grant TED2021-129679B-C22.

References

1 W. L. Barnes, S. A. R. Horsley and W. L. Vos, Classical Antennas, Quantum Emitters, and, Densities of Optical States, *J. Opt.*, 2020, **22**, 073501.
2 K. H. Drexhage, Influence of a Dielectric Interface on Fluorescence Decay Time, *J. Lumin.*, 1970, **1–2**, 693–701.
3 K. H. Drexhage, H. Kuhn and F. P. Schäfer, Variation of the Fluorescence Decay Time of a Molecule in Front of a Mirror, *Bunsen-Ges. Phys. Chem., Ber.*, 1968, **72**, 329–329.
4 D. Geng, E. Cabello-Olmo, G. Lozano and H. Míguez, Tamm Plasmons Directionally Enhance Rare-Earth Nanophosphor Emission, *ACS Photonics*, 2019, **6**, 634–641.
5 D. Geng, E. Cabello-Olmo, G. Lozano and H. Míguez, Photonic Structuring Improves the Colour Purity of Rare-Earth Nanophosphors, *Mater. Horiz.*, 2018, **5**, 661–667.

6 D. Englund, D. Fattal, E. Waks, G. Solomon, B. Zhang, T. Nakaoka, Y. Arakawa, Y. Yamamoto and J. Vučković, Controlling the Spontaneous Emission Rate of Single Quantum Dots in a Two-Dimensional Photonic Crystal, *Phys. Rev. Lett.*, 2005, **95**, 013904.
7 J. M. Viaña, M. Romero, G. Lozano and H. Míguez, Nanoantennas Patterned by Colloidal Lithography for Enhanced Nanophosphor Light Emission, *ACS Appl. Nano Mater.*, 2022, **5**, 16242–16249.
8 J. A. Schuller, E. S. Barnard, W. Cai, Y. C. Jun, J. S. White and M. L. Brongersma, Plasmonics for Extreme Light Concentration and Manipulation, *Nat. Mater.*, 2010, **9**, 193–204.
9 A. Jiménez-Solano, J. F. Galisteo-López and H. Míguez, Absorption and Emission of Light in Optoelectronic Nanomaterials: The Role of the Local Optical Environment, *J. Phys. Chem. Lett.*, 2018, **9**, 2077–2084.
10 O. L. Muskens, V. Giannini, J. A. Sánchez-Gil and J. Gómez Rivas, Strong Enhancement of the Radiative Decay Rate of Emitters by Single Plasmonic Nanoantennas, *Nano Lett.*, 2007, **7**, 2871–2875.
11 T. Senden, F. T. Rabouw and A. Meijerink, Photonic Effects on the Radiative Decay Rate and Luminescence Quantum Yield of Doped Nanocrystals, *ACS Nano*, 2015, **9**, 1801–1808.
12 S. F. Wuister, C. De Mello Donegá and A. Meijerink, Local-Field Effects on the Spontaneous Emission Rate of CdTe and CdSe Quantum Dots in Dielectric Media, *J. Chem. Phys.*, 2004, **121**, 4310–4315.
13 E. He, H. Zheng, X. Zhang and S. Qu, Local-Field Effect on the Fluorescence Relaxation of Tm^{3+}:LaF_3 Nanocrystals Immersed in Liquid Medium, *Luminescence*, 2010, **25**, 66–70.
14 X. Xue, T. Suzuki, H. T. Tong and Y. Ohishi, Investigation of Local Field Effect of α-$NaYF_4$:Nd^{3+} Nanocrystals, *Phys. Status Solidi C*, 2012, **9**, 2481–2484.
15 K. Dolgaleva, R. W. Boyd and P. W. Milonni, *Influence of Local-Field Effects on the Radiative Lifetime of Liquid Suspensions of Nd:YAG Nanoparticles*, 2007.
16 R. S. Meltzer, S. P. Feofilov, B. Tissue and H. B. Yuan, Dependence of Fluorescence Lifetimes of Y_2O_3:Eu^{3+} Nanoparticles on the Surrounding Medium, *Phys. Rev. B: Condens. Matter Mater. Phys.*, 1999, **60**, R14012–R14015.
17 C. K. Duan and M. F. Reid, Macroscopic Models for the Radiative Relaxation Lifetime of Luminescent Centers Embedded in Surrounding Media, *Spectrosc. Lett.*, 2007, **40**, 237–246.
18 K. K. Pukhov, T. T. Basiev and Y. V. Orlovskii, Spontaneous Emission in Dielectric Nanoparticles, *JETP Lett.*, 2008, **88**, 12–18.
19 D. Toptygin, Effects of the Solvent Refractive Index and Its Dispersion on the Radiative Decay Rate and Extinction Coefficient of a Fluorescent Solute, *J. Fluoresc.*, 2003, **13**, 201–219.
20 Y. Luo, L. Li, H. T. Wong, K. Wong and P. A. Tanner, Importance of Volume Ratio in Photonic Effects of Lanthanide–Doped $LaPO_4$ Nanocrystals, *Small*, 2020, **16**(1), 1905234.
21 C. Feldmann, Luminescent Nanomaterials, *Nanoscale*, 2011, **3**, 1947.
22 J. F. Galisteo-López and G. Lozano, Nanophotonics for Current and Future White Light-Emitting Devices, *J. Appl. Phys.*, 2021, **130**, 200901.
23 B. Casabone, C. Deshmukh, S. Liu, D. Serrano, A. Ferrier, T. Hümmer, P. Goldner, D. Hunger and H. de Riedmatten, Dynamic Control of Purcell Enhanced Emission of Erbium Ions in Nanoparticles, *Nat. Commun.*, 2021, **12**, 3570.
24 A. P. Moneda and D. P. Chrissoulidis, Dyadic Green's Function of a Cluster of Spheres, *J. Opt. Soc. Am. A*, 2007, **24**, 3437.
25 C. Van Vlack and S. Hughes, Finite-Difference Time-Domain Technique as an Efficient Tool for Calculating the Regularized Green Function: Applications to the Local-Field Problem in Quantum Optics for Inhomogeneous Lossy Materials, *Opt. Lett.*, 2012, **37**, 2880.
26 A. Jiménez-Solano, J. F. Galisteo-López and H. Míguez, Fine Tuning the Emission Properties of Nanoemitters in Multilayered Structures by Deterministic Control of Their Local Photonic Environment, *Small*, 2015, **11**, 2727–2732.
27 K. A. Ivanov, K. M. Morozov, G. Pozina, A. R. Gubaydullin, E. I. Girshova and M. A. Kaliteevski, Control of the Surface Plasmon Dispersion and Purcell Effect at the Metamaterial-Dielectric Interface, *Sci. Rep.*, 2020, **10**, 20828.
28 L.-W. Li, P.-S. Kooi, M.-S. Leong and T.-S. Yee, Electromagnetic Dyadic Green's Function in Spherically Multilayered Media, *IEEE Trans. Microwave Theory Tech.*, 1994, **42**, 2302–2310.
29 J. Humlicek, Data Analysis for Nanomaterials: Effective Medium Approximation, Its Limits and Implementations, in *Ellipsometry at the Nanoscale*, Springer Berlin Heidelberg, Berlin, Heidelberg, 2013, pp. 145–178.
30 D. Geng, G. Lozano and H. Míguez, Highly Efficient Transparent Nanophosphor Films for Tunable White-Light-Emitting Layered Coatings, *ACS Appl. Mater. Interfaces*, 2019, **11**, 4219–4225.
31 A. Rubino, G. Lozano, M. E. Calvo and H. Míguez, Determination of the Optical Constants of Ligand-Free Organic Lead Halide Perovskite Quantum Dots, *Nanoscale*, 2023, **15**, 2553–2560.
32 Z. Wang, T. Senden and A. Meijerink, Photonic Effects for Magnetic Dipole Transitions, *J. Phys. Chem. Lett.*, 2017, **8**, 5689–5694.
33 R. Martín-Rodríguez, F. T. Rabouw, M. Trevisani, M. Bettinelli and A. Meijerink, Upconversion Dynamics in Er^{3+}-Doped Gd_2O_2S: Influence of Excitation Power, Er^{3+} Concentration, and Defects, *Adv. Opt. Mater.*, 2015, **3**, 558–567.
34 J. W. Stouwdam and F. C. J. M. Van Veggel, Near-Infrared Emission of Redispersible Er^{3+}, Nd^{3+}, and Ho^{3+} Doped LaF_3 Nanoparticles, *Nano Lett.*, 2002, **2**, 733–737.
35 N. S. Singh, R. S. Ningthoujam, N. Yaiphaba, S. D. Singh and R. K. Vatsa, Lifetime and Quantum Yield Studies of

Dy^{3+} Doped $GdVO_4$ Nanoparticles: Concentration and Annealing Effect, *J. Appl. Phys.*, 2009, **105**, 064303.

36 M. Yu, J. Lin and J. Fang, Silica Spheres Coated with YVO_4:Eu^{3+} Layers via Sol-Gel Process: A Simple Method to Obtain Spherical Core-Shell Phosphors, *Chem. Mater.*, 2005, **17**, 1783–1791.

37 M. Inokuti and F. Hirayama, Influence of Energy Transfer by the Exchange Mechanism on Donor Luminescence, *J. Chem. Phys.*, 1965, **43**, 1978–1989.

38 M. Buijs, A. Meyerink and G. Blasse, Energy Transfer between Eu^{3+} Ions in a Lattice with Two Different Crystallographic Sites: Y_2O_3:Eu^{3+}, Gd_2O_3:Eu^{3+} and Eu_2O_3, *J. Lumin.*, 1987, **37**, 9–20.

39 K. Lu, W. Han, G. Cheng, X. Zhu, S. Li, H. Guo, B. Gu, Y. Ye, J. Qi and T. Lu, Dy^{3+}-Doped $Y_2Zr_2O_7$ Highly Transparent Ceramics for Ultraviolet Excitable Warm White Light-Emitting Applications, *J. Am. Ceram. Soc.*, 2023, **106**(6), 3654–3662.

40 G. Mialon, S. Türkcan, A. Alexandrou, T. Gacoin and J. P. Boilot, New Insights into Size Effects in Luminescent Oxide Nanocrystals, *J. Phys. Chem. C*, 2009, **113**, 18699–18706.

41 D. V. Guzatov, S. V. Gaponenko and H. V. Demir, Possible Plasmonic Acceleration of LED Modulation for Li-Fi Applications, *Plasmonics*, 2018, **13**, 2133–2140.

42 T. Tsutsui, M. Yahiro, H. Yokogawa, K. Kawano and M. Yokoyama, Doubling Coupling-out Efficiency in Organic Light-Emitting Devices Using a Thin Silica Aerogel Layer, *Adv. Mater.*, 2001, **13**, 1149–1152.

43 V. Baranau and U. Tallarek, Random-Close Packing Limits for Monodisperse and Polydisperse Hard Spheres, *Soft Matter*, 2014, **10**, 3826.

44 N. O. Nuñez, S. Rivera, D. Alcantara, J. M. de la Fuente, J. García-Sevillano and M. Ocaña, Surface Modified Eu:$GdVO_4$ Nanocrystals for Optical and MRI Imaging, *Dalton Trans.*, 2013, **42**, 10725.